Chapter 6

Multiplicity fluctuation and forward-backward multiplicity correlation

6.1 Introduction

The multiparticle emission data obtained from the RHIC and LHC experiments have inspired many to investigate the fluctuations of particle densities in nuclear collisions, and to examine the rapid formation of QGP that expands hydrodynamically with very low specific viscosity [1, 2]. The initial density fluctuations are found to transfer very efficiently into collective flow correlations in the momentum space. Experimental measurement of such correlations provide us therefore, with an opportunity to look into the space-time evolution of the collective expansion as well as the medium properties that drives such expansion. Observables like e-by-e fluctuations of the charged hadron multiplicity, fluctuations of dynamical variables like the total transverse momentum (p_t) or total rapidity (y) of particles per event, and correlations among these particles, are often used as statistical tools for such kind of investigations. The equation of state of the fireball matter is sensitive to the above mentioned fluctuation and correlation measures. The initial state density fluctuations are also studied in the longitudinal direction [3]. The longitudinal fluctuations are directly related to the entropy production at the early stages of the collision, well before the onset

of the collective flow, and in terms of the multiplicity of produced particles they appear as long-range correlations well separated in the rapidity (y) or pseudorapidity (η) space. On the other hand, short-range correlations are usually generated through resonance decays, jet fragmentation and Bose-Einstein correlations. The short-range correlations are localized over a relatively smaller range of y or η, and are sensitive to the final-state effects. Recently short range correlations between two hard knocked nucleons has been studied by using the inverse kinematics in the Baryonic Matter at Nuclotron (BM@N) experiment conducted at the Nuclotron-based Ion Collider (NICA) facility at Joint Institute of Nuclear Research at Dubna, Russia [4]. The results have significant implications in nuclear, high-energy and astro-particle physics.

In this chapter we report some results on the short and long-range longitudinal correlations, and e-by-e fluctuations of charged particle multiplicities. The observables of our interest are the correlation among singly charged particles emitted in the forward and backward hemispheres of the η-space [5], a roughness parameter associated with the η-distributions of the singly charged particles produced [6], the scaled variance of charged particles [7, 8], and an e-by-e fluctuation measure of the charged particle multiplicities [9, 10]. We analyze the particle emission data obtained from ^{16}O-Ag/Br and ^{32}S-Ag/Br interactions at an incident beam energy of 200A GeV. Following the trend of our analysis we systematically compare the experimental results with the UrQMD simulation [11, 12]. The Bose-Einstein correlation (BEC), considered to be the major source of short-range correlations among identical bosons, has been mimicked into our simulated data sample(s) as an after-burner by using a charge reassignment algorithm [13]. The objectives are, (i) to study the longitudinal dynamics of short and long-range particle correlations generated by the density fluctuations at the early stages of collisions, (ii) to confirm the presence of dynamical fluctuations in the particle emission data by using standard statistical methods, (iii) to set a reference baseline for the experimental measures by using a hadronic transport model like the UrQMD, (iv) to examine the degree of mismatch between the experiment(s) and simulation(s), and (v) to check if that can be compensated by mimicking the BEC into our simulated data.

6.2 Literature review

Large density of particles produced within a narrow region of η is traditionally called a spike, which was first observed by the JACEE collaboration in very high-energy cosmic-ray events [14]. Since that observation several statistical techniques have been developed, some of which are already discussed in the previous chapters of this thesis, to understand the spike structures in the pseudorapidity distributions of JACEE events. However, a systematic comparison of the experimental density fluctuations with model simulations may

bring out some useful information related to multiparticle production [6, 15–17]. While large multiplicity fluctuations could be a signal of particle production via clusters [18] or super-cooled droplets of QCD matter [19], small fluctuations in the final state of conserved charges, electric or baryonic, are seen when the fluctuations generated in the plasma phase are frozen due to rapid expansion of the fireball system [20]. It was found that if the hot and dense fireballs hadronize near the critical QCD end-point, significant transverse momentum and multiplicity fluctuations would be observed [21]. In this line the lattice calculations are presented in [20, 21]. The results on electric charge and transverse momentum fluctuations, particularly in terms of the Φ-measure [9, 10], are presented in [22, 23]. Though, on several occasions the Φ-measure is used to quantify the p_t and net-charge fluctuations only [24–26], in this analysis we have used it to measure the fluctuations in the η-space.

In several studies on the forward-backward (FB) correlation of particle multiplicities like in e^+e^- [27], pp [28–31] and AB [32, 33] collisions, significant correlation between the forward and backward multiplicities have been observed. The PHOBOS collaboration at RHIC have studied the FB multiplicity correlation in Au+Au interaction at $\sqrt{s_{NN}} = 200$ GeV [32]. Aziz *et al.* [34] proposed a model to extract the effective cluster multiplicity $K_{\rm eff}$ from the PHOBOS data. The $K_{\rm eff}$-values were found to be 2.2 for the $0--20\%$ centrality, and 2.7 for the $40--60\%$ centrality intervals. These values surely exceed the prediction of a hadron resonance gas (HRG) model which reported $K_{\rm eff} \approx 1.5$ [35]. The STAR Au+Au collision results at top RHIC energy showed that the FB correlation strength decreases rapidly from central to peripheral interactions [33]. The UrQMD prediction matches the RHIC Au+Au data for the peripheral collisions while the model overestimates the experimental results for the central collisions. The HIJING model however, exhibits an opposite behavior of the UrQMD [36]. Recently, a study on multiplicity correlations has been generalized by decomposing the correlation function into orthogonal Legendre polynomial functions, more generally into the principal components, each representing a unique component of the measured FB correlation [37, 38]. Particle production in pp collisions is usually described by the QCD-inspired models like PYTHIA [39] and EPOS [40]. Previous studies show that these models can grossly describe the pseudorapidity and transverse momentum dependence of the inclusive charged-particle spectra [41], as well as the underlying dynamics accompanying various hard-scattering processes [42]. In many such models, events with large charged-particle multiplicities are produced through several multi-parton interactions (MPI), which naturally serves as sources for the FB multiplicity asymmetry described above. Presence of long-range FB correlation has been predicted in the Dual Parton model (DPM) and in the Color Glass Condensate (CGC)/Glasma model [43, 44], both of which contain one form of the color flux tubes or the other, e.g. color strings in the DPM and Glasma flux tubes in the CGC, that actually lead to long-range correlations [45].

6.3 Roughness in η-distribution

A standard χ^2 test has been performed to investigate the roughness present in the single particle pseudorapidity distributions. The method has been elaborated in [6]. Accordingly, if n_{ik} is the number of shower tracks emitted in the i-th η-bin of the k-th event, $\langle n_i \rangle = N_{\rm ev}^{-1} \sum_k n_{ik}$ is the event sample averaged multiplicity in the i-th bin, and $n_k = \sum_i n_{ik}$ is the corresponding multiplicity of the k-th event, then the χ^2 value for the k-th event is defined as,

$$\chi_k^2 = \sum_{i=1}^{M} \left(n_{ik} - \langle n_i \rangle\right)^2 / \sigma_{ik}^2 \tag{6.1}$$

Here M is the number of η-bins and $\sigma_{ik} = \sqrt{n_{ik}}$ is the statistical error associated with n_{ik}. χ_k^2 is sensitive to the e-by-e fluctuations in the shower track multiplicity per event with respect to its event sample averaged value $\langle n_k \rangle$. Therefore, another variable γ_k^2, which depends only on the shape of the single particle η-distribution, is introduced as,

$$\gamma_k^2 = \sum_{i=1}^{M} \left(n_{ik} - \frac{n_k}{\langle n_k \rangle} \langle n_i \rangle\right)^2 / \sigma_{ik}^2 \tag{6.2}$$

γ_k^2 measures the roughness of the η-distribution function. A large value of γ_k^2 implies that n_{ik} is far from its event sample mean $\langle n_i \rangle$, thereby denoting a probable cluster of particles. In the above $\langle\ \rangle$ denotes an averaging over the entire event sample.

The probability distributions of γ_k^2 for our experiments are compared with the respective UrQMD simulations in Figure 6.1. The presence of spikes, i.e. high probabilities of finding

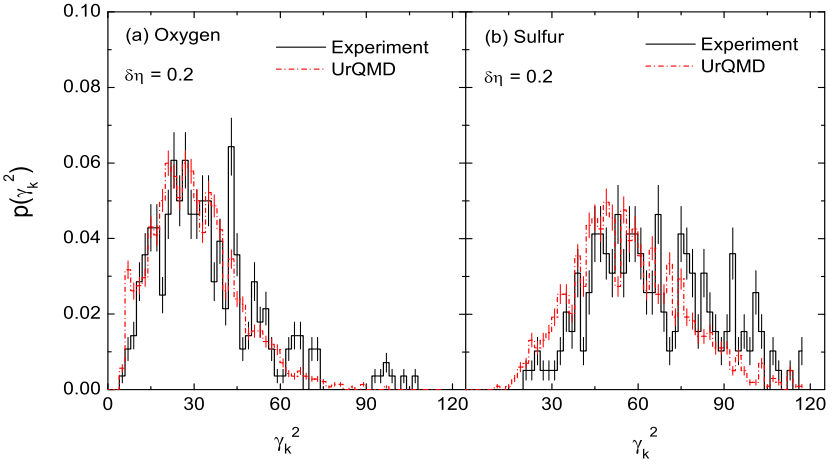

Figure 6.1: Distributions of γ_k^2 for pseudorapidity bin $\delta\eta = 0.2$.

γ_k^2-values within a narrow $\delta\eta$, as well as valleys are quite prominent in these distributions. In particular, spikes are seen in several places in the large γ_k^2-region of each experimental

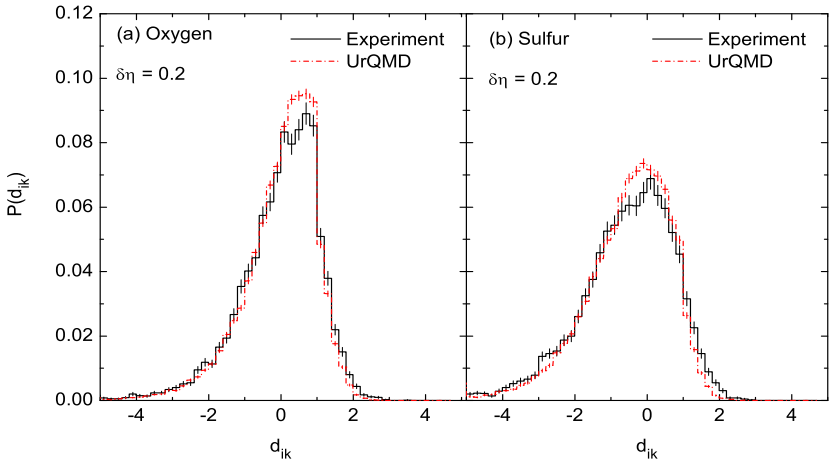

Figure 6.2: Distributions of d_{ik} for pseudorapidity bin $\delta\eta = 0.2$.

distribution, which the corresponding simulation could not match. Such fluctuations may arise due to (a) statistical reasons, (b) kinematic constraints, (c) BEC between identical particles, or (d) some non-trivial dynamics associated with multiparticle production. The mean and standard deviation values of the γ_k^2-distributions are calculated for two pseudorapidity bin widths i.e. $\delta\eta = 0.1$ and 0.2, and their values are listed in Table 6.1. We see that the $\langle\gamma_k^2\rangle$ and $\sigma(\gamma_k^2)$-values for the experiment are consistently greater than, though not significantly different from, the simulated values. For both the interactions the UrQMD+BEC simulations yield slightly larger values of parameters than the UrQMD generated values. There is an indication that by mimicking BEC into our simulations we may to some extent, though not completely, account for the particle correlations. The $\langle\gamma_k^2\rangle$ and $\sigma(\gamma_k^2)$ values calculated for $\delta\eta = 0.1$ are higher than the corresponding values obtained for $\delta\eta = 0.2$. A larger η-window perhaps smooths out the roughness present in the e-by-e fluctuation. In this regard an obvious and significant projectile mass dependence in the results is observed from Table 6.1. We next find out large local densities of particles that correspond to large entropy contained within small domains of η-space. The parameter [6],

$$d_{ik} = \left(n_{ik} - \frac{n_k}{\langle n_k\rangle}\langle n_i\rangle\right)/\sigma_{ik} \tag{6.3}$$

measures the deviation in the particle number from its event average in the i-th bin of width $\delta\eta$ of the k-th event, and therefore, it also measures the fluctuation in the local density of particle number. The probability distributions of d_{ik} for the ^{16}O-Ag/Br and ^{32}S-Ag/Br experimental data are compared schematically with the respective simulations in Figure 6.2. We have noted that in terms of the single particle distributions, the UrQMD and UrQMD+BEC predictions are quite identical. Therefore, in this diagram only the UrQMD generated distributions are plotted against the respective experiment. For both

Table 6.1: The values of $\langle\gamma_k^2\rangle$ and $\sigma(\gamma_k^2)$ for the ^{16}O- and ^{32}S-induced Ag/Br interactions at 200A GeV/c. The values are calculated for pseudorapidity window $\delta\eta = 0.2$ and 0.1.

	^{16}O-Ag/Br		^{32}S-Ag/Br	
Data	$\langle\gamma_k^2\rangle$	$\sigma(\gamma_k^2)$	$\langle\gamma_k^2\rangle$	$\sigma(\gamma_k^2)$
$\delta\eta = 0.2$				
Experiment	34.58±1.09	18.26±0.77	66.38±1.61	23.47±1.13
UrQMD	30.41±0.39	14.74±0.74	57.55±0.66	20.15±0.47
UrQMD+BEC	31.19±0.42	15.73±0.29	59.28±0.60	20.83±0.42
$\delta\eta = 0.1$				
Experiment	39.17±1.33	22.26±0.77	83.40±2.24	31.71±1.58
UrQMD	36.33±0.51	19.20±0.74	78.72±1.07	30.35±0.71
UrQMD+BEC	37.91±0.37	19.91±0.37	79.67±0.59	30.67±0.59

types of interactions probability distributions of d_{ik} are smooth and slightly left-skewed. The simulated distribution functions, perhaps due to their larger statistics, are smoother than the respective experimental distribution. In the peak region of the distribution of each type of interaction, the UrQMD prediction slightly exceeds the experiment. The experiment and the simulated data do not otherwise differ very significantly.

6.4 Forward-backward multiplicity correlation

In high-energy collisions multiparticle production takes place mainly through two different classes of sub-processes. One of them consists of soft processes that can be explained in terms of multiple parton interactions at low p_t. Processes of this kind are often characterized by correlations in the local particle number density $\rho(\eta) = N_{\rm ev}^{-1}\,(dn_{\rm ch}/d\eta)$ that usually extends over a long η-range [46]. On the other hand, at high p_t values hard perturbative processes like radiative transitions or parton scattering take place through single and/or a few-parton exchange. These processes generate particle jets, which by definition are characterized by short-range correlations. Such processes are associated with high multiplicity, found typically within a unit of η or so, and quickly diminish with increasing η-gap. Thus a soft process results in a smaller particle multiplicity with weaker correlation prevailing over a wider η-separation, the so-called long-range correlation. In comparison, hard processes result in a small number of jets that are characterized by a high multiplicity within a small η-interval, the so called short-range correlation. As the p_t value increases above a few hundred MeV, there is a gradual transition from the soft to the hard processes. Therefore, particle correlations examined as a function of separation in the η-space and η-interval size, can be used to measure the contribution of each category of sub-processes mentioned above. Forward-backward (FB) correlation measure as a function of rapidity (y) or pseudorapidity

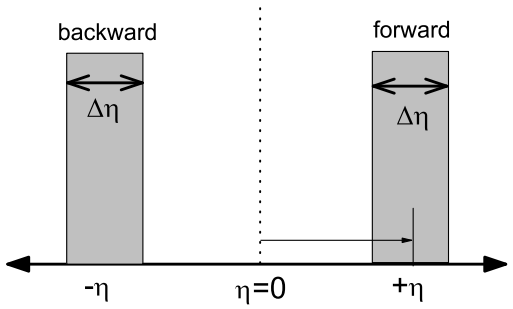

Figure 6.3: A schematic diagram showing how the forward and backward windows are selected in η-distribution.

(η) can be used to examine the longitudinal characteristics of the fireball system produced in high-energy AB interactions.

We consider two η-windows of width $\Delta\eta$ each at positions $\pm\eta$, located symmetrically about the centroid of the overall η-distribution of the event sample. A schematic diagram in Figure 6.3 describes the above consideration. Let the number of charged particles in the forward window be denoted by n_f and that in the backward window be denoted by n_b. For correlated emission of particles, one observes the following linear dependence [47],

$$\langle n_b \rangle = a + b\, n_f \tag{6.4}$$

Here b is a measure of the correlation strength. The FB-correlation is also measured in terms of a FB-asymmetry parameter (C) defined as,

$$C = \frac{n_f - n_b}{\sqrt{n_f + n_b}} \tag{6.5}$$

The variance of charged particle multiplicities is then given by $D_{qq} = \langle n_q^2 \rangle - \langle n_q \rangle^2$, where $q = f$ for the forward and $q = b$ for the backward window, and $\langle\ \rangle$ stands for an averaging over the event sample. The covariance of n_f and n_b is defined as $D_{fb} = \langle n_f\, n_b \rangle - \langle n_f \rangle \langle n_b \rangle$. The fluctuation in C can be expressed in terms of the variance and covariance of the asymmetry parameter as [5],

$$\sigma_c^2 = \frac{D_{ff} + D_{bb} - 2D_{fb}}{\langle n_f + n_b \rangle} \tag{6.6}$$

In principle σ_c^2 should have contributions from both short and long-range correlations [34]. The short-range contribution comes from particle production due to cluster decay. A cluster in general can be a resonance state, a partonic jet or a QGP droplet. When $\Delta\eta$ is larger than the cluster size, all particles belonging to the cluster should be within that interval. The long-range contribution on the other hand, comes perhaps from the fragmentation of stretched color strings or color flux tubes that may be extended over a longer y or η-range. If the bins centered around $\pm\,\eta$ are largely separated in the η-axis, contribution of long-range

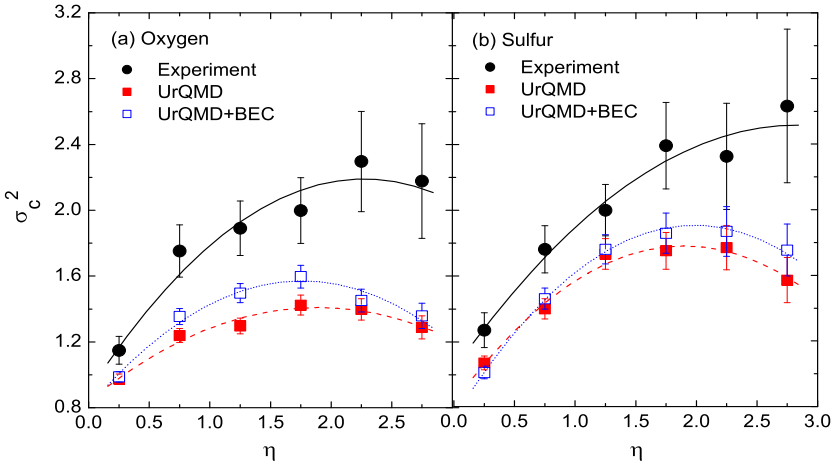

Figure 6.4: σ_c^2 as a function of pseudorapidity η measured about the centroid of the η-distribution. Continuous curves are drawn to visualize the trend of the data points.

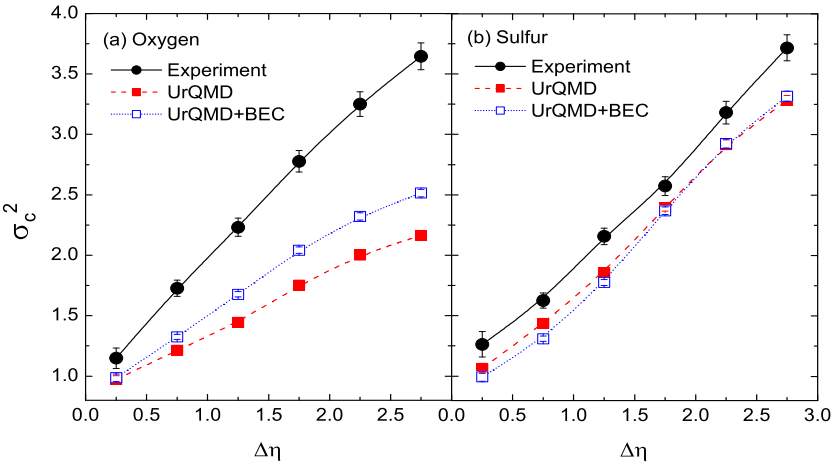

Figure 6.5: σ_c^2 as a function of pseudorapidity windows $\Delta\eta$ at $\eta = \pm 1.5$ about the centroid of the η-distribution. Continuous curves are drawn to visualize the trend of the data points.

correlation becomes negligibly small. Only under such circumstances one can approximate as $\sigma_c^2 \approx K_{\text{eff}}$, where K_{eff} is the effective multiplicity in a cluster. The correlation strength parameter b can also be obtained in terms of the covariance as [48],

$$b = D_{fb}/D_{ff} \tag{6.7}$$

In the absence of any correlation among the particles, when the covariance D_{fb} is vanishing, or when the separation between forward and backward windows is very large, the dynamical correlation approaches its Poisson limit. In either case $\sigma_c^2 \approx K_{\text{eff}} = 1$, which indicates no cluster.

We calculate fluctuations in the FB-multiplicity asymmetry (σ_c^2) as functions of η and $\Delta\eta$. The results are graphically shown respectively in Figures 6.4 and 6.5, where we consider a

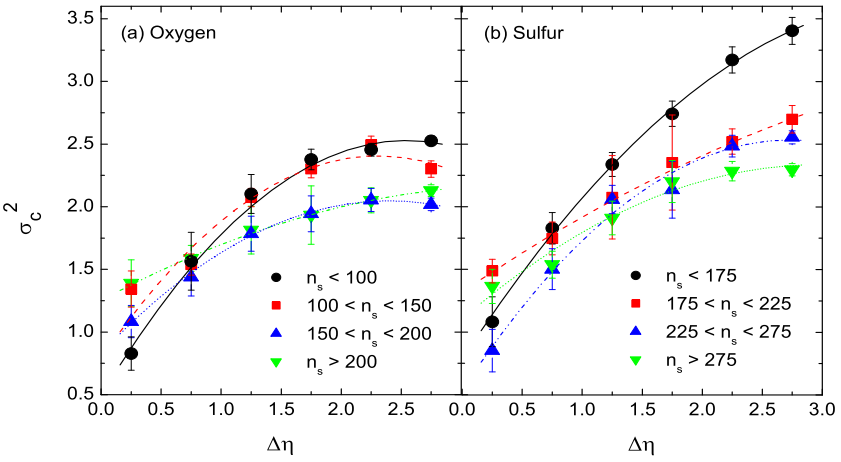

Figure 6.6: σ_c^2 as a function of pseudorapidity windows $\Delta\eta$ at $\eta = \pm 1.5$ about the centroid of the η-distribution for four different multiplicity classes. Continuous curves are drawn to visualize the trend of the data points.

pair of η-bins each of equal width $\Delta\eta$ located symmetrically at $\pm\eta$ about the centroid η_0 of the overall distribution. In Figure 6.4 we then vary the η-value keeping window size fixed at $\Delta\eta = 0.5$. Whereas in Figure 6.5 overlapping η-windows of varying width are taken at a fixed separation $|\eta - \eta_0| = 1.5$. In Figure 6.4 we see that for each type of interaction the experimental value of σ_C^2 starts from $\sigma_c^2 \approx 1.2$ at $\eta = 0.25$, it grows with increasing η-gap up until $\eta \approx 2.0$ units or so, and then attains a kind of saturation, e.g. at $\sigma_c^2 \approx 2.0$ in the ^{16}O-Ag/Br and at $\sigma_c^2 \approx 2.4$ in the ^{32}S-Ag/Br interaction. On the other hand, the UrQMD and the UrQMD+BEC generated values are initially found to increase with increasing η, attain maximum in the intermediate stage before finally dropping down to some extent at the end. Perhaps due to hadronic rescattering embedded into the UrQMD model, the initial fluctuations present in the FB-correlation are to some extent destroyed at large η. The simulated values of σ_c^2 are significantly smaller than the experiment, the difference being larger in ^{16}O-Ag/Br interaction than in the ^{32}S-Ag/Br interaction. Inclusion of BEC into the UrQMD model, though statistically not very significant, slightly enhances the values of σ_c^2. In Figure 6.4 we also see a definite system size dependence. The values of σ_c^2 in ^{32}S-Ag/Br interaction are consistently higher than the corresponding values obtained from the ^{16}O-Ag/Br interaction. Moreover, the saturation as mentioned above, has perhaps been attained a little earlier in the ^{16}O-Ag/Br interaction than in the^{32}S-Ag/Br interaction. Figure 6.5 shows that σ_c^2 increases linearly with increasing $\Delta\eta$ over almost the entire range under consideration ($0.25 \leq \Delta\eta \leq 2.75$). Once again we see that the simulated values are consistently lower than the experiment in both cases. In the ^{32}S-Ag/Br interaction the model predictions are to some extent closer to the experiment than that in the ^{16}O-Ag/Br interaction. Absence of any kind of saturation in these plots indicates that all correlated particles could not be accommodated even within the widest $\Delta\eta$ considered.

This observation perhaps indicate presence of long-range correlations in the η-space. In order to reduce the effects of widely varying collision geometry, to the extent it is possible within a limited statistics that is typical to an emulsion experiment, we have divided each experimental event sample into four sub-samples by using the shower track multiplicity cuts. In Figure 6.6 only the experimental σ_c^2 values are plotted against $\Delta\eta$ at a fixed gap $|\eta - \eta_0| = 1.5$. The general nature of the variation in σ_c^2 with $\Delta\eta$, as we see in these plots, is quite different from that of the Figure 6.5. At higher $\Delta\eta$ ($\approx 2.0 - 2.5$) the σ_c^2 values attain saturation. We may therefore conclude that the linear rise observed in Figure 6.5 is nothing but a trivial artifact originating from varying collision geometry. As expected, we observe that in both the interactions considered, the fluctuation measures, particularly at large $\Delta\eta$, are smaller in more central events. The overall nature of our data is almost similar to that observed in the peripheral (40-60% central) Au+Au collisions [49]. Our results indicate that the particle production in both interactions are so correlated that cannot be matched with the UrQMD model. Inclusion of BEC in the simulation does not make any significant change in the outcome either.

In Figure 6.7 we plot the correlation strength b against η-gap for a fixed window size $\Delta\eta = 0.5$. Equation (6.7) is used to determine b. We see that in ^{16}O-Ag/Br interaction the

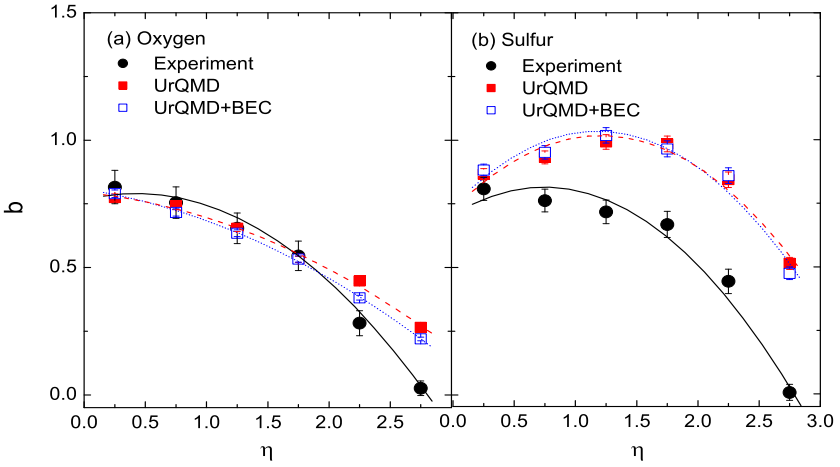

Figure 6.7: Plot of forward-backward correlation parameter b as a function of pseudorapidity gap η. Continuous curves are drawn to visualize the trend of the data points.

correlation strength monotonically decreases with increasing gap between η-windows located in the forward and backward hemispheres. In ^{32}S-Ag/Br interaction the variation of b with η is almost similar to that of the ^{16}O-Ag/Br interaction. Both the model predictions are very close to the experiment in the ^{16}O-Ag/Br case except for the largest gap $\eta = 2.75$. In the ^{32}S-Ag/Br case the simulations however significantly exceed the experiment and remain relatively flat over a comparatively larger η-range. This can be interpreted

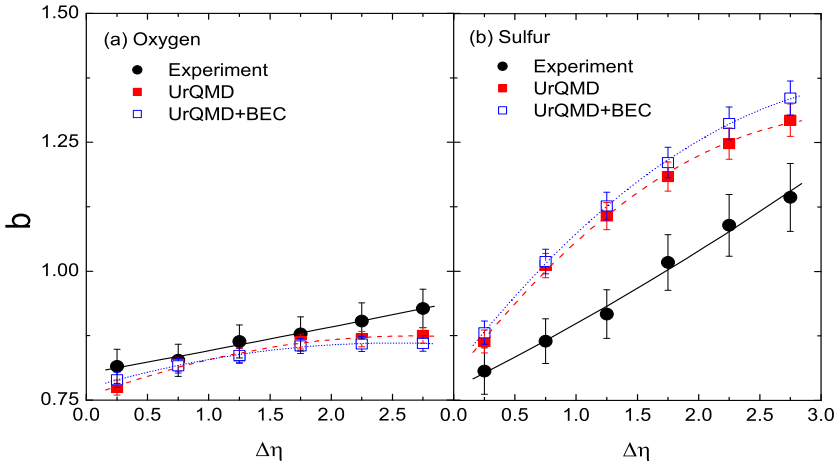

Figure 6.8: b parameter plotted against pseudorapidity window size $\Delta\eta$. Continuous curves are drawn to visualize the trend of the data points.

in terms of long-range correlations present in the ^{32}S-Ag/Br simulation data, for which the string fragmentation and transport mechanisms like diffusion present in the UrQMD model may be held accountable. The hadronic rescattering embedded in the UrQMD may not be strong enough to melt the cluster structure. In Figure 6.8 we plot the correlation strength against $\Delta\eta$ for a fixed η-gap. We see that in both ^{16}O-Ag/Br and ^{32}S-Ag/Br interactions the experimental b-values increase linearly with $\Delta\eta$, while the corresponding simulations exhibit some kind of saturation at large $\Delta\eta$. The linear rise is sharper in ^{32}S-Ag/Br interaction than in the ^{16}O-Ag/Br interaction. Once again, while in the ^{16}O-Ag/Br interaction the simulations approximately reproduce the experiment, in the ^{32}S-Ag/Br case they significantly exceed the experiment. It seems that the fireballs produced in the latter interaction are in general closer to equilibrium, and therefore, thermodynamically more random in nature.

6.5 ω-measure

As mentioned above, a QGP to hadron phase transition may give rise to large rapidity and multiplicity fluctuations of produced particles and have distinct effects on the dynamics or the space-time evolution of the fireball. One way to measure the multiplicity fluctuations is to use the scaled variance (ω) of the maultiplicity distribution. ω is defined as [7, 8],

$$\omega = \frac{\mathrm{Var}(n)}{\langle n\rangle} = \frac{\langle n^2\rangle - \langle n\rangle^2}{\langle n\rangle} \tag{6.8}$$

where $\mathrm{Var}(n) = \sum_k (n_k - \langle n\rangle)^2\, P(n_k)$ and $\langle n\rangle = \sum_k n_k\, P(n_k)$ are respectively the variance and mean of the multiplicity distribution $P(n_k)$. For an independent particle emission, i.e

for a purely statistical mechanism $P(n_k)$ follows Poisson distribution which results in $\omega = 1$. We measure the η-dependence of ω for the shower tracks and show the results schematically

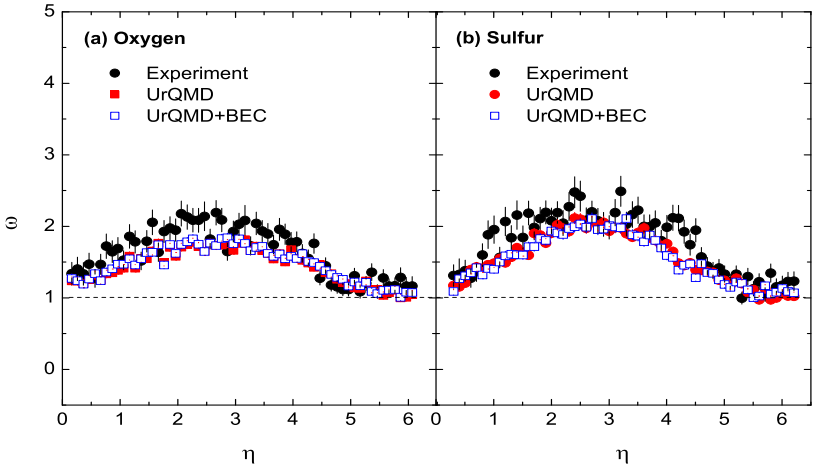

Figure 6.9: Pseudorapidity dependence of the scaled variance ω of the multiplicity distribution.

in Figure 6.9. For comparison the UrQMD and UrQMD+BEC simulated results are also included in the same graph. For both ^{16}O-Ag/Br and ^{32}S-Ag/Br interactions the ω versus η plot looks like a bell-shaped distribution within $0 \leq \eta \leq 6$. The ω-values are almost always greater than their Poisson limit except for $\eta \geq 5$, where the ω-value tends to saturate towards its Poisson limit. In both interactions the experimental values of ω are marginally greater than the corresponding UrQMD and/or UrQMD+BEC predication. However, under no circumstances the difference between the experiment and simulation is so significant as to augment any excess fluctuation typically required near a critical point. Figure 6.9 reflects the presence of particle correlations in the experimental data as well as in the model simulations. The degree of correlation, i.e. deviation from the Poisson limit is maximum in the central η-region ($2.5 \leq \eta \leq 3.5$) in the experiments as well as in the simulations. The charge reassignment algorithm implemented into the UrQMD simulation, does not affect the ω-measure significantly. In a rather detailed analysis of the NA49 data, it is seen that UrQMD can approximately reproduce the energy as well as the rapidity dependence of the ω-values associated with the charge hadron multiplicity in Pb+Pb collisions at 20A and 158A GeV incident beam energies [50].

6.6 Φ-measure

The Φ-measure of net-charge fluctuation was introduced in [9, 10]. The observable Φ potentially removes the trivial statistical contributions and determines the dynamical e-by-e

fluctuations. The definition of Φ is not limited to measure the net-charge fluctuation only, but it is also applicable to dynamical variables like p_t, y and/or η. Following [9, 10] we define the deviation in the variable x_i from its inclusive mean $\overline{x}$ as, $\Delta x_i = x_i - \overline{x}$. In our case for the i-th shower track $x_i \equiv \eta_i$. By definition the mean $\overline{\Delta x} = 0$, and the mean square deviation is $\overline{\Delta x^2} = \overline{(x_i - \overline{x})^2}$. Analogously for each event the deviation is introduced as,

$$\Delta X = \sum_{i=1}^{n_k} \Delta x_i \tag{6.9}$$

where n_k is the number of shower tracks (particles) present in the k-th event. The Φ_η-measure is then defined as,

$$\Phi_\eta = \sqrt{\frac{\langle \Delta X^2 \rangle}{\langle n \rangle}} - \sqrt{\overline{\Delta x^2}} \tag{6.10}$$

Here $\langle\ \rangle$ denotes an event averaging. In absence of any inter-particle correlation $\Phi_\eta \to 0$. Moreover, the fluctuation measure Φ_η would be independent of the number of particle producing sources provided the sources are identical and independent, and provided an AB collision can be treated as an incoherent superposition of many such sources.

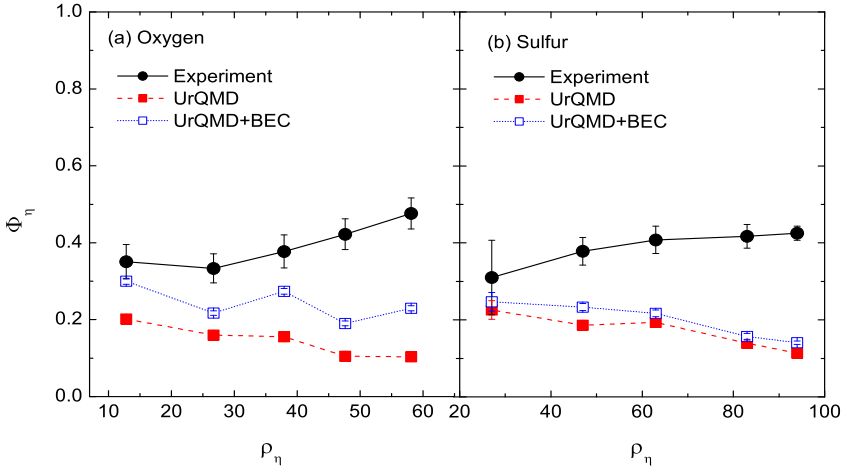

Figure 6.10: The values of Φ_η-measure are shown as a function of pseudorapidity density ρ_η.

The centrality dependence of Φ_η is shown in Figure 6.10. The centrality is measured in terms of the central pseudorapidity density of the produced particles $\rho_\eta = N_{\rm ev}^{-1}\,(dn/d\eta)\,|_{\eta_0}$. For both the experiments Φ_η values are found to slowly and marginally increase with increasing ρ_η. For both interactions the experimental Φ_η-values vary within a narrow range ($\sim 0.30 - 0.45$). In the ^{32}S-Ag/Br case, beyond $\rho_\eta = 60$ the Φ_η-values remain almost unchanged, indicating a dominance of independent particle producing sources in semicentral and central events. There is a definite indication of particle correlations being present in

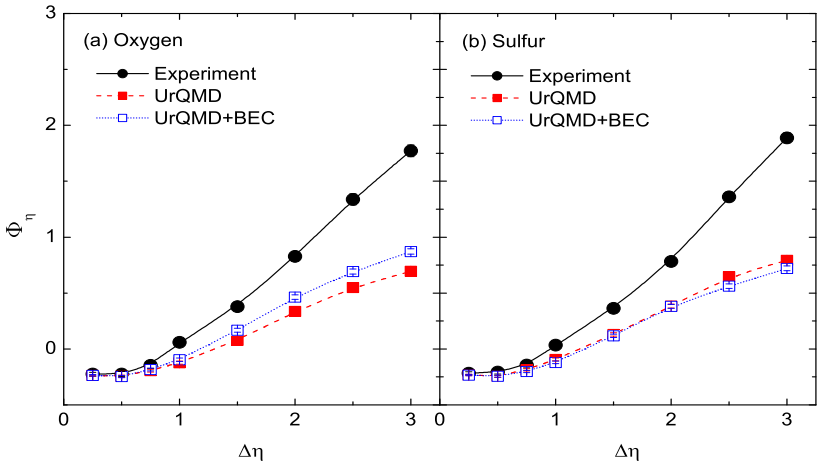

Figure 6.11: The values of Φ_η measure are shown as a function of overlapping pseudorapidity window $\Delta\eta$

both the experimental data samples. The strength of correlation at least in the ^{16}O-Ag/Br events, increases as one moves from peripheral to central collisions. In contrast, the UrQMD simulated values are consistently smaller than the corresponding experimental values. The simulated values show slightly decreasing trend with increasing ρ_η. This implies that the Φ_η measure is sensitive even to the correlations present in the UrQMD model, originating mainly due to resonance decays, jet fragmentation etc. The hadronic re-scattering effect present in the model, might have diluted the correlation to some extent at more central collisions having large particle densities. The BEC effect adds some extra correlation to the UrQMD simulation, which is more prominent in the ^{16}O-Ag/Br case than in the ^{32}S-Ag/Br case. The $\Delta\eta$-dependence of Φ_η is shown in Figure 6.11. In both experiments we see that beyond $\Delta\eta = 1.0$ the fluctuation measure Φ_η is positive, it increases almost linearly with increasing $\Delta\eta$, and its variation is almost independent of the mass number of the projectile nucleus. The simulated values of Φ_η on the other hand are consistently smaller than the respective experiment, and their rise with increasing $\Delta\eta$ is also not as sharp as they are in the experiments. The differences between the UrQMD and UrQMD+BEC simulations are not very significant in either case. Φ_η is negative valued below $\Delta\eta = 1.0$ in both the experiments and in the corresponding simulations, which should be attributed to lack of correlation due to a small size of the phase-space interval, some of the correlated particles may have been excluded. Even the kinematic conservation laws may not be valid for such a limited interval.

6.7 Summary

The forward-backward multiplicity correlations and e-by-e fluctuations in various correlation measures have been investigated by using two sets of nuclear emulsion data on ^{16}O-Ag/Br and ^{32}S-Ag/Br interactions at an incident beam energy of 200 GeV/nucleon. The experimental results are compared with the UrQMD simulation, as well as with the UrQMD simulation modified with a charge reassignment algorithm that mimics the Bose-Einstein correlation. In spite of the limitations regarding the statistics, which is typical to any emulsion experiment, we have been able to make several important observations, which are summarized below.

1. The roughness distribution of particles are examined through a χ^2 test, and large concentrations of particles within small η-intervals are observed that cannot be reproduced by the UrQMD and UrQMD+BEC simulations. On some occasions the particle densities are too large to be merely due to statistical reasons or kinematic constraints.

2. Fluctuations in the forward-backward asymmetry parameter show dominance of short-range correlation in the pseudorapidity space, which in the ^{16}O-Ag/Br interaction gets diluted to some extent. However, in the ^{32}S-Ag/Br interaction the correlation strength sustains even at the large η-gaps as well as in large $\Delta\eta$. Small sized clusters are responsible for the short-range correlations observed. The UrQMD simulation, even after inclusion of the BEC effect, can not reproduce the experimental results. At large η re-scattering among hadrons significantly dilutes the fluctuation observed. Inclusion of the BEC marginally improves the simulation results.

3. Our observation on the correlation strength parameter is more or less consistent with that of the fluctuations observed in the FB asymmetry parameter. While the UrQMD and UrQMD+BEC simulations can almost predict the ^{16}O-Ag/Br experiment, they significantly over predict the ^{32}S-Ag/Br results. In the latter case it seems that in the experiment, inter-particle correlations are more susceptible to the fireball environment than what has been assumed in the simulation.

4. Presence of particle correlations is reaffirmed through the ω-measure. Non-Poissonian multiplicity distribution within small η-interval is established through this test. The experimental results however are very close to the simulations which do not warrant any critical phenomenon.

5. The Φ_η-measure of dynamical fluctuations indicate that both ^{16}O-Ag/Br and ^{32}S-Ag/Br collision events can perhaps be approximated as incoherent superpositions of many binary NN collisions. Hadronic re-scattering dilutes the simulated values to noticeable extent.

The statistical tools used in this analysis have their own limitations [51], and the AB collision events have a widely varying geometry. The results presented in this analysis however certainly indicate that the mechanism of particle production in UrQMD is in no way sufficient to describe the real dynamics of AB interactions.

Bibliography

[1] H. Song, Euro. Phys. J. A 48, 163 (2012).

[2] W. Busza, K. Rajagopal and W. van der Schee, Ann. Rev. Nuc. Part. Sci. 68, 1 (2018).

[3] M. Gaździcki, M. I. Gorenstein and S. Mrówczyński, Phys. Lett. B 585, 115 (2004).

[4] A. Galavanov *et al.*, J. Phys: Conf. Series, 1390, 012025 (2019).

[5] B. B. Back *et al.* (UA5 Collaboration), Z. Phys C 37, 191 (1998).

[6] M. Cherry *et al.* (KLM Collaboration), Acta Phys. Pol. B 29, 2129 (1998).

[7] V. V. Begun *et al.*, Phys. Rev. C 70, 034901 (2004).

[8] B. Lungwitz and M. Bleicher, Phys. Rev. C 76, 044904 (2007).

[9] M. Gaździcki and S. Mrówczyński, Z. Phys. C 54, 127 (1992).

[10] S. Mrówczyński, Phys. Lett. B 465, 8 (1999).

[11] S. A. Bass *et al.,* Prog. Part. Nucl. Phys. 41, 255 (1998).

[12] M. Bleicher *et al.*, J. Phys. G 25, 1859 (1999).

[13] O. V. Utyuzh, G. Wilk and Z. Wlodarczyk, Phys. Lett. B 522, 273 (2001).

[14] T. H. Burnett *et al.* (JACEE Collaboration), Phys. Rev. Lett. 50, 2062 (1962).

[15] B. Wosiek (KLMM Collaboration), Proc.XXV Int. Symp. on Multiparticle Dynamics, World Scientific (1996) p.271.

[16] P. Deines-Jones *et al.* (KLM Collaboration), Phys. Rev. C 53, 3044 (1996).

[17] G. Roland *et al.* (PHOBOS Collaboration), Nucl. Phys. A 774, 113 (2006).

[18] E. V. Shuryak, Nucl. Phys. A 715, 289 (2003).

[19] G. Baym and H. Heiselberg, Phys. Lett. B 469, 7 (1999).

[20] S. Jeon and V. Koch, Phys. Rev. Lett. 85, 2076 (2000);
M. Asakawa, U. Heinz, and B. Müller, Phys. Rev. Lett. 85, 2072 (2000).

[21] N. G. Antoniou *et al.*, Phys. Lett. B 432, 8 (1998).

[22] C. Alt *et al.* (NA49 Collaboration), Phys. Rev. C 70, 064903 (2004).

[23] T. Anticic *et al.* (NA49 Collaboration), Phys. Rev. C 70, 034902 (2004).

[24] G. Roland (for the NA49 Collaboration), Nucl. Phys. A 638, 91c (1998);
H. Appelshauser *et al.* (NA49 collaboration), Phys. Lett. B 459, 679 (1999).

[25] M. Bleicher *et al.*, Phys. Lett. B 435, 9 (1998).

[26] A. Capella, E. G. Ferreiro and A. B. Kaidalov, Euro. Phys. J. C 11, 163 (1999).

[27] W. Braunschweig *et al.* (TASSO Collaboration), Z. Phys. C 45, 193 (1989).

[28] S. Uhlig, I. Derado, R. Meinke and H. Preissner, Nucl. Phys. B 132, 15 (1978).

[29] R. Ansorge *et al.* (UA5 Collaboration), Z. Phys. C 37, 191 (1988).

[30] ATLAS Collaboration, J. High Energy Phys. 07, 019 (2012).

[31] J. Adam *et al.* (ALICE Collaboration), J. High Energy Phys. 05, 097 (2015).

[32] B. B. Back *et al.* (PHOBOS Collaboration), Phys. Rev. C 74, 011901(R) (2006).

[33] B. I. Abelev *et al.* (STAR Collaboration), Phys. Rev. Lett. 103, 172301 (2009).

[34] M. Abdel-Aziz and M. Bleicher, arXiv:nucl-th/0605072.

[35] M. Stephanov, K. Rajagopal and E. Shuryak, Phys. Rev. D 60, 114028 (1999).

[36] S. Haussler, M. Abdel-Aziz and M. Bleicher, Nucl. Phys. A 785, 253c (2007).

[37] A. Bzdak and D. Teaney, Phys. Rev. C 87, 024906 (2013).

[38] R. S. Bhalerao *et al.,* Phys. Rev. Lett. 114, 152301 (2015).

[39] T. Sjöstrand *et al.,* Comput. Phys. Commun. 178, 852 (2008).

[40] T. Pierog *at al.*, Phys. Rev. C 92, 034906 (2015).

[41] G. Aad *et al.* (ATLAS Collaboration), Phys. Lett. B 758, 67 (2016);
M. Aaboud *et al.* (ATLAS Collaboration), Eur. Phys. J. C 76, 502 (2016).

[42] G. Aad *et al.* (ATLAS Collaboration), Eur. Phys. J. C 74, 2965, *ibid* 3195 (2014).

[43] A. Capella and J. T. T. Van, Phys. Lett. B 93, 146 (1980); Z. Phys. C 10, 249 (1981).

[44] T. Lappi and L. McLerran, Nucl. Phys. A 772, 200 (2006).

[45] T. J. Tarnowsky (STAR Collaboration), Proceedings of the 22nd Winter Workshop on Nuclear Dynamics, California, USA (2006).

[46] W. Kittel and E. A. de Wolf, Soft Multihadron Dynamics, World Scientific (2005).

[47] S. Lim, Y. Lim, C. Oh and K. Phua, Z. Phys. C 43, 621 (1989).

[48] A. Capella, U. Sukhatme, C.-I. Tan and J. T. T. Van, Phys. Rep. 236, 225 (1994).

[49] G. Roland (NA49 Collaboration), Proc. of the Quark Matter 1997, Japan (1997).

[50] C. Alt *et al.* (NA49 Collaboration), Phys. Rev. C 78, 034914 (2008).

[51] O. V. Utyuzh, G. Wilk and Z. Wlodarczyk, Phys. Rev. C 64, 027901 (2001).